IEEE Access
Multidisciplinary | Rapid Review | Open Access Journal

Received 9 January 2023, accepted 8 February 2023, date of publication 13 February 2023, date of current version 16 February 2023.

Digital Object Identifier 10.1109/ACCESS.2023.3244608

RESEARCH ARTICLE

Center Frequency Tracking Scheme to Optimize Pulse-Echo Response of Ultrasonic A-mode Scanner Circuit System

DOO-HYEON KO, YOUNG-CHAN LEE, AND JI-YONG UM, (Member, IEEE)
Department of Medical IT Convergence Engineering, Kumoh National Institute of Technology, Gumi 39253, South Korea

Corresponding author: Ji-Yong Um (jyum@kumoh.ac.kr)

This work was supported in part by the Basic Science Research Program through the National Research Foundation (NRF) of Korea funded by the Ministry of Education under Grant 2019R1I1A3A01060591; in part by the Commercialization Promotion Agency for Research and Development Outcomes (COMPA) through the Korea Government (MSIT) under Grant 2021I100; in part by the Korea Institute for Advancement of Technology (KIAT) through the Korea Government (MOTIE) under Grant P0017011.

ABSTRACT This paper proposes a center frequency tracking scheme to optimize a pulse-echo response of ultrasonic A-mode scanner. A pulse-echo response of A-mode scanner represents an overall energy conversion characteristic from an actuation to an acquisition. A center frequency for optimized pulse-echo response can be varied depending on an actuation voltage, an acoustic medium, etc. Most of previous frequency tracking methods have focused on high-power continuous actuation applications, and have relied on a monitoring of phase difference between actuating voltage and current with auxiliary sensors. This work focuses on a monitoring of a peak envelope of echo without additional sensors. We employ a momentum based gradient ascent algorithm along with a finite state machine to track an optimum center frequency so that a peak envelope of echo becomes the maximum value. The proposed frequency tracking scheme was implemented on a field programmable gate array for real-time operation. We performed repetitive measurements to verify consistent frequency tracking performances for different acoustic mediums. The A-mode scanner adaptively tracked corresponding center frequencies for each of mediums within an average error of 61.7 kHz. When the A-mode scanner was in a steady state, an increment of signal-to-noise ratio (SNR) of echo was 7.4 dB, and an axial resolution was improved by 32.5 %.

INDEX TERMS Center frequency tracking, A-mode ultrasound, gradient-ascent algorithm, momentum optimization, finite state machine, field programmable gate array, A-mode scanner circuit system.

I. INTRODUCTION

An A-mode ultrasound scanner represents an amplitude-mode pulsed ultrasound device. It transmits a pulsed ultrasound with several number of cycles with a center frequency, and receives an acoustic echo signal during relatively long time to surrogate impedance characteristics of medium. Since an ultrasonic A-mode scanner is based on a single transducer element, it has a potential to be applied for wearable or portable devices such as a medical diagnosis, a hand-gesture recognition, and a non-destructive evaluation [1], [2], [3], [4], [5].

A procedure of transmission and acquisition of ultrasound is one of representative energy conversion between electrical domain and mechanical domain. An energy conversion efficiency between different domains can be primarily affected by various conditions such as an actuation voltage, a center frequency, a pulse shape, and an impedance matching [6], [7], [8], [9], [10], [11], [12], [13], [14], [15], [16]. These conditions are related to a nature of ultrasound transducer.

Previous works for high-power continuous actuation of transducer have focused on a conditioning of resonance state [6], [7], [8], [9], [10], [11]. That is, a primary goal was

The associate editor coordinating the review of this manuscript and approving it for publication was Yiming Huo.

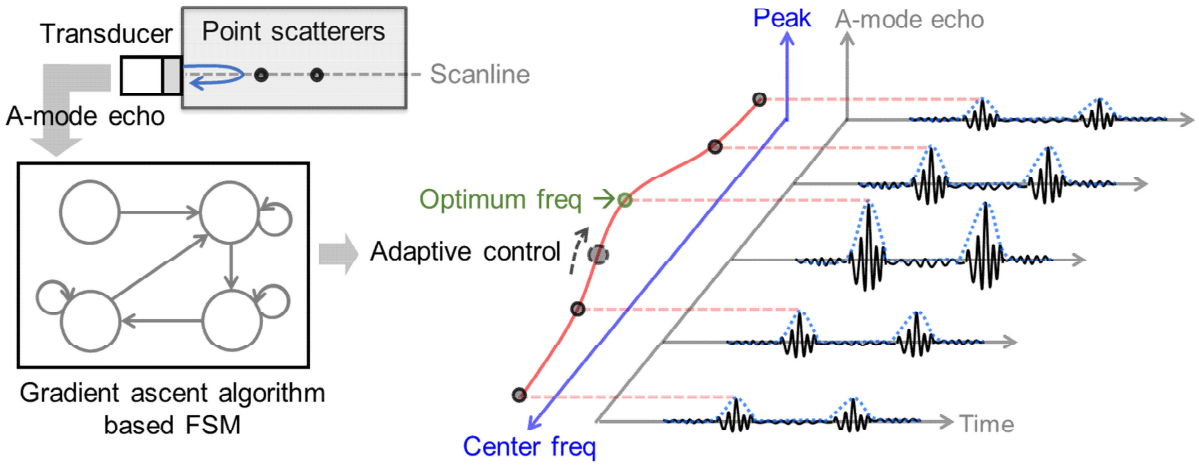

FIGURE 1. Concept of proposed center frequency tracking scheme for A-mode scanner.

to make a transducer impedance lowest and purely resistive so that the impedance phase becomes zero. This aim can be mostly achieved by means of an impedance matching and a resonance frequency tracking scheme. Phase-locked loops (PLLs) were widely employed to adjust a phase difference between actuation voltage and current. However, previous works of [6], [7], [8], [9], [10], and [11] needed additional current sensors for phase monitoring. Also, the aforementioned works only considered continuous actuations without receiving echo signals. In addition, frequency ranges were less than MHz range. Hence, the aforementioned works cannot be directly utilized for A-mode scanner with a center frequency of few MHz.

Other previous works for high-energy efficiency in actuation of transducer have focused on pulse shapes [12], [13], [14], [15], [16]. These works can be categorized to low-energy transmission compared with works of [6], [7], [8], [9], [10], and [11], and were implemented as a form of application specific integrated circuits (ASICs). Target transducers of [12], [13], [14], [15], and [16] were micro-electro-mechanical systems (MEMS), and the corresponding frequency was few MHz range. These works employed tri-level or multi-level pulsing for enhanced energy efficiency. The aforementioned works paid little attention on an optimum center frequency, even though a deviation of center frequency of MEMS based transducer is not negligible [17], [18], [19]. In addition, a center frequency of transducer along with quality factor can vary depending on an input power, an ambient temperature, and an acoustic loading condition of medium [6], [7], [8], [9], [10], [20]. Considering actual instrumentations, an overall energy-conversion efficiency can be further improved if a real-time center frequency tracking method is employed properly.

In this paper, we propose a center frequency tracking scheme to optimize a pulse-echo response of A-mode scanner (Fig. 1). An improvement of pulse-echo response implies that an overall energy conversion from transmission to acquisition is improved. The proposed scheme monitors a peak amplitude of echo envelope. Then, it tracks a center frequency so that the peak value of envelope becomes the maximum without use of additional sensors (Fig. 1). The proposed center frequency tracking scheme is based on the gradient ascent algorithm, and the algorithm is implemented as a digital circuit system for a real-time operation. The proposed scheme enhances a signal-to-noise ratio (SNR) and an axial resolution of A-mode scanner.

A frequency response of typical transducer can be simplified as a parabolic curve with a global maximum [9], [10], [21]. A conceptual illustration in Fig. 1 also shows a concave curve with a global maximum. In actual instrumentations, a frequency response of transducer can have several local maximums or non-strongly concave points at the vicinity of the optimum frequency. In this paper, we consider a low-Q-factor transducer, which has a good axial resolution compared with a high-Q-factor transducer. A curvature in frequency response of low-Q-factor transducer is relatively small. Then, a gradient around the optimum frequency is also small, and a global maximum tracking can be subject to noise in measurement setup. So, we adopt a concept of momentum based gradient ascent algorithm, which can reach the global maximum point by avoiding local maximum or non-strongly concave points robustly [22], [23], [24], [25].

A concept of momentum based gradient ascent algorithm is implemented as one of states of finite state machine (FSM) on a field programmable gate array (FPGA). When the FSM updates a center frequency with the momentum based gradient method, a center frequency gradually approaches a target frequency by avoiding non-strongly concave points. After frequency tracking, an envelope of A-mode echo can be maximized. Besides, the proposed scheme can track the corresponding center frequencies consistently for different acoustic mediums.

The paper is organized as follows. Section II describes the architecture of proposed frequency tracking scheme. In Section III, implementation and measurement results are presented. Then, the conclusions are described in Section IV.

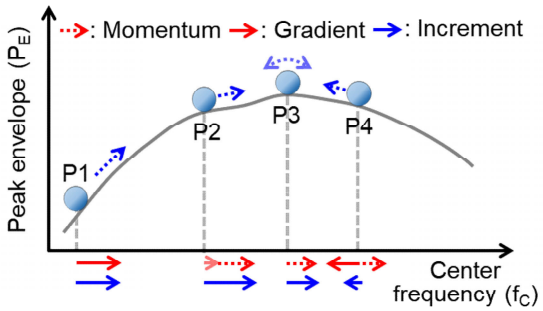

FIGURE 2. Concept of proposed center frequency tracking with momentum based gradient ascent algorithm.

II. CENTER FREQUENCY TRACKING IN ULTRASONIC A-MODE SCANNER CIRCUIT SYSTEM

In this section, we will describe the proposed center frequency tracking based on gradient ascent algorithm. The frequency control is performed by using FSM. Conditions for each of states in FSM is determined with criteria of momentum of frequency increment. The relevant analysis for momentum and pre-measured frequency response will be presented. In addition, since one of aims of this work is to implement a real-time stand-alone A-mode scanner, an architecture of overall ultrasonic A-mode scanner circuit system along with its operation will be described.

A. CENTER FREQUENCY TRACKING SCHEME

The gradient based optimization algorithms are widely utilized in learning procedures of machines or systems [22], [23], [24], [25], [26], [27]. To accomplish a robust tracking of maximum or minimum value of cost function, concepts of stochastics or momentums are combined in gradient based optimizations [22], [23], [24], [25]. We have a similar optimization problem to estimate the global maximum point in a frequency response of A-mode scanner. Fig. 2 shows a conceptual frequency response of ultrasonic A-mode scanner. Note that the frequency response of Fig. 2 has a parabolic curve with one non-strongly concave point, and the vertical axis corresponds to a peak amplitude of envelope in A-mode echo signal during a single pulse repetition interval (PRI). Depending on several conditions such as an impedance matching and a quality factor of transducer, a non-strongly concave point in the vicinity of optimum center frequency can appear.

To estimate the global maximum point in frequency response robustly, we adopt a momentum based gradient ascent algorithm as shown in Fig. 2. A concept of momentum represents a tendency of moving object to keep its moving nature, and a momentum is proportional to a velocity vector. The velocity vector can be defined as a derivative of a coordinate with respect to time. In this context, a center frequency of this work can be understood as a coordinate in concept of momentum. Then, a center frequency can be expressed as below [27].

$$f_C[n] = f_C[n-1] + \gamma v[n-1] + \eta \frac{\partial P_E}{\partial f_C} \qquad (1)$$

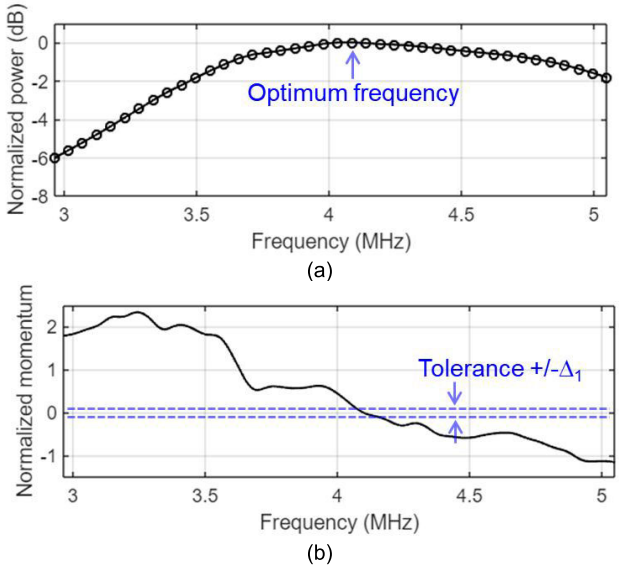

FIGURE 3. (a) Normalized power of A-mode echo envelope with respect to center frequency of ultrasonic A-mode scanner (b) estimated momentum by using measured frequency response.

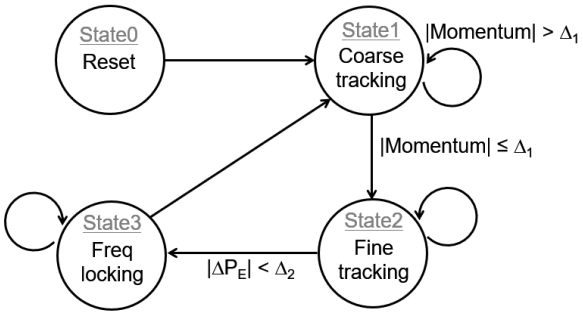

FIGURE 4. FSM diagram for center frequency tracking.

where $f_C[n]$, $v[n]$, γ, P_E, η are a center frequency, a velocity, a momentum term, a peak amplitude of envelope, and a learning rate in a discrete domain.

The center frequency of (1) is incremented by both of the momentum of $\gamma \cdot v[n\text{-}1]$ and the gradient term $\eta \cdot \partial P_E/\partial F_C$. Fig. 2 illustrates four example points of $P1$, $P2$, $P3$, and $P4$. The point $P1$ represent the initial beginning point, and its increment is only determined by the gradient. The frequency increment of each point, $P2$, $P3$, and $P4$, corresponds to a net vector of momentum and gradient. If the point $P2$ has a sufficient momentum, the frequency increment can be enough to escape a non-strongly concave point even though the instantaneous gradient is zero. In actual instrumentations, the frequency update can be stuck for a while or longer time around the non-strongly concave point due to a temporal noise. Thanks to a momentum, a center frequency $f_C[n]$ can be dithered around the global maximum in a steady state.

To accomplish a smooth convergence of center frequency, we need to properly decrement the weighting parameters of γ and η as the center frequency approaches the optimum point. So, we monitor the momentum and to check whether the momentum is within the pre-determined tolerance or not.

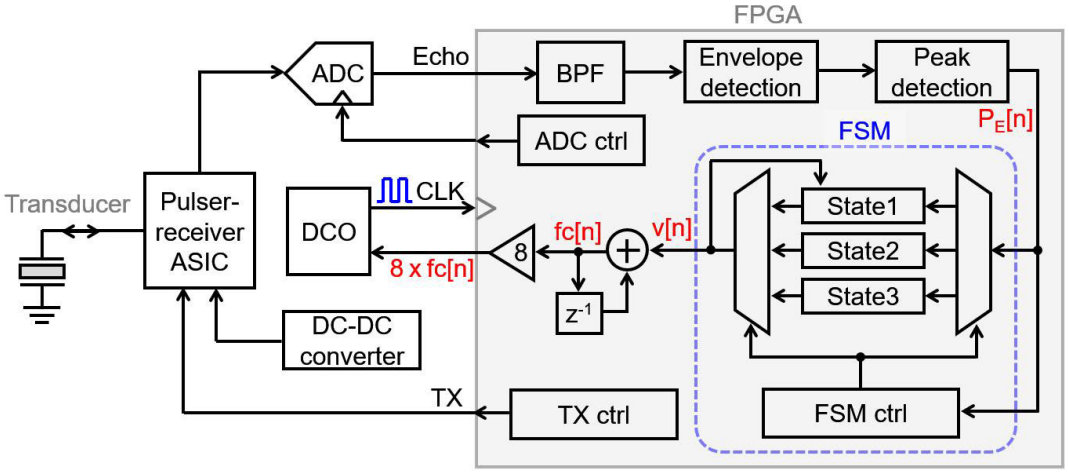

FIGURE 5. Block diagram of ultrasonic A-mode scanner circuit system with center frequency tracking scheme.

If the momentum is within the tolerance, then the state of circuit system is altered to adjust the weighting parameters.

In this work, we pre-estimate the tolerance of momentum through a relevant analysis. The frequency increment of Δf_C in (1) can be rewritten as below.

$$v[n] = \gamma v[n-1] + \eta \left[\frac{\partial P_E}{\partial f_C}\right]_n \tag{2}$$

The velocity $v[n]$ of (2) is equivalently an accumulation of exponentially weighted past gradients. Considering the initial condition, then the velocity of (2) can be expressed as below.

$$v[n] = \eta \sum_{i=1}^{n} \gamma^{n-i} \left[\frac{\partial P_E}{\partial f_C}\right]_i \tag{3}$$

Fig. 3(a) illustrates the measured normalized power of A-mode echo envelope with respect to the center frequency. The envelope response of Fig. 3(a) corresponds the response of transfer function of pulse-echo system. Note that the transfer function of pulse-echo system can be modelled with an overall convolution of impulse responses from the transmitter to the receiver parts including energy conversion efficiency. The frequency response of Fig. 3(a) provides several insights for an overall design flow. That is, we can preliminarily check the optimal center frequency of pulse-echo system and features of response curve such as the global maximum point and gradient characteristics. Besides, we can derive requirements for circuit implementation as well. The frequency response of Fig. 3(a) can be used to estimate the momentum by using (3), and the corresponding result is shown in Fig. 3(b). As mentioned before, the momentum corresponds to an accumulation of weighted past gradients, so it shows a decreasing tendency due to a concave shape of the frequency response. Also, the estimated momentum becomes sufficiently small around the optimum center frequency. By using this feature, we set the tolerance value Δ_1 for state transition.

Fig. 4 shows the FSM diagram for proposed center frequency tracking scheme. There are four states: *Reset* state (State0), *Coarse tracking* state (State1), *Fine tracking* state (State2), and *Freq locking* state (State3). After a global reset, the state of system becomes *Coarse tracking* state. In this state, the system performs the frequency tracking by means of momentum based gradient ascent method, which follows (1). When the center frequency approaches the global maximum point of frequency response, the absolute of momentum $\gamma \cdot v[n\text{-}1]$ is dithered within the tolerance Δ_1 during the certain time duration. Then, the state is altered to *Fine tracking* state. In this state, the momentum term γ is set to zero, and the learning rate η is set to smaller value for fine frequency tracking. That is, the State2 follows a basic gradient-ascent algorithm. When the center frequency value $f_C[n]$ is finely close to the optimum value, the derivative of peak envelope $P_E[n]$ becomes sufficiently small within a resolution of system. Then, the state is altered to *Freq locking* state. In this state, the center frequency value $f_C[n]$ is not updated, and kept to be a constant value. When the condition for State3 is not satisfied during the certain time, then the system re-starts the frequency tracking from State1. This is because the system regards that the optimum center frequency conditions such as acoustic mediums, pulsing voltages, or pulse shapes are suddenly changed. The center frequency value $f_C[n]$ considering the FSM diagram of Fig. 4 can be expressed as below.

$$v[n] = \begin{cases} \eta_1 \sum_{i=1}^{n} \gamma^{n-i} \left[\frac{\partial P_E}{\partial f_C}\right]_i, & at\ State1 \\ \eta_2 \frac{\partial P_E}{\partial f_C}, & at\ State2 \\ 0, & at\ State3 \end{cases} \tag{4}$$

B. ULTRASONIC A-MODE SCANNER

Fig. 5 shows a block diagram of ultrasonic A-mode scanner circuit system with center frequency tracking scheme. It consists of a single-element ultrasonic transducer, a FPGA, a pulser-receiver ASIC, an analog-to-digital converter (ADC), a digitally controlled oscillator (DCO), and a DC-DC converter. The pulser-receiver ASIC includes a programmable bipolar pulser, a transmit/receive switch, and a programmable-gain amplifier [28]. The ASIC proceeds

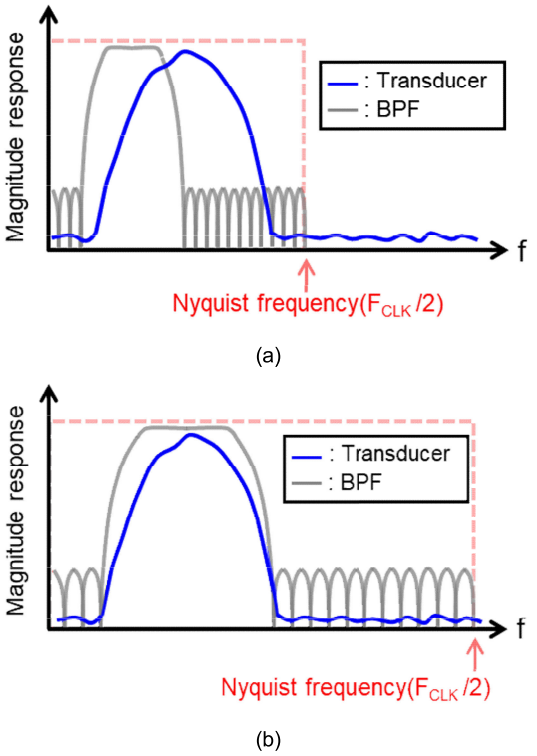

FIGURE 6. Intrinsic frequency response of transducer and stretchable frequency response of BPF (a) initial state (b) steady state.

periodic actuations and acquisitions of ultrasound, and its operation is controlled by FPGA. The conditioned analog echo signal is fed into the discrete chip ADC, and the digitized signal *Echo* is delivered into FPGA for digital processing. The discrete chip DCO generates the signal *CLK*, which acts as the system clock of FPGA. The frequency of DCO is controlled by FPGA, and its value is eight times of the center frequency value $f_C[n]$.

The architecture of FPGA is comprised of echo conditioning blocks, an FSM, an accumulator as a loop filter, and other control logics. The FSM operates based on the diagram of Fig. 4, and the frequency increment $v[n]$ is implemented to satisfy the equation (4). The computations in FSM are not complicated since most of computations are based on accumulation.

The echo conditioning blocks in FPGA are a BPF, an envelope detection, and a peak detection. The type of BPF is a finite impulse response (FIR) filter, and the order of BPF is 45. The quality factor of filter is around 1.1, and the center frequency of the passband is 1/8 of the sampling frequency. Note that the sampling frequency is equal to the system clock frequency F_{CLK}. Basically, the BPF has a role to suppress out-of-band noise. In addition, the BPF of this work affects the efficiency of echo acquisition.

The fractional bandwidth of BPF with respect to the sampling frequency is fixed due to hardwired coefficients of filter. As a result, in the initial state, the frequency of system clock is set to the minimal value, and accordingly the passband of BPF

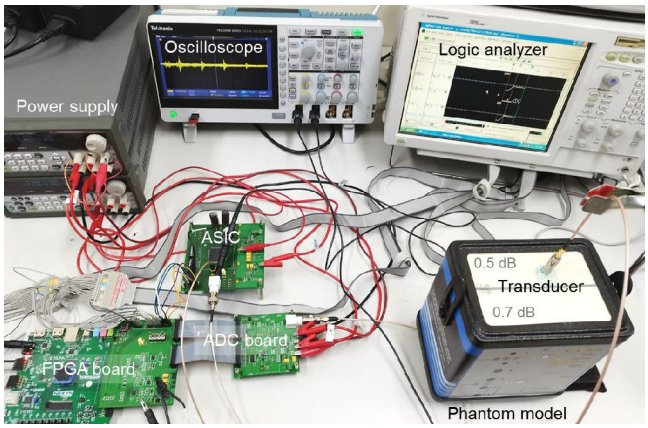

FIGURE 7. Measurement setup.

TABLE 1. Summary of FPGA resource utilization.

	Value	Available	Utilization
LUTs	2325	133800	1.74 %
DSP slices	40	740	5.41 %
Slice registers	1109	267600	0.41 %
BRAM (18 kB)	0.0	365	0.00 %

TABLE 2. Summary of transducer impedance analysis.

	0.5 dB/(MHz·cm)	0.7 dB/(MHz·cm)
R_l	5.9 Ω	7.6 Ω
L_l	237 nH	251 nH
C_l	6.37 nF	6.59 nF
C_0	56.0 pF	56.2 pF
f_r	4.115 MHz	3.941 MHz
$\mu[f_C]$	4.054 MHz	3.886 MHz
$\sigma[f_C]$	23.9 kHz	25.4 kHz

is also shrunk due to low Nyquist frequency (Fig. 6(a)). Then, the equivalent passband performance is deteriorated due to insufficient overlap of frequency responses of transducer and BPF. As the frequency tracking proceeds, the passband of BPF is stretched and the effective passband performance is gradually improved. When the optimum center frequency is tracked at the steady state, then the effective passband from the transducer to the BPF is optimized, and the efficiency of echo acquisition is also maximized (Fig. 6(b)). Therefore, the center frequency tracking of this work not only estimates the optimal actuation frequency but also to find the optimal sampling frequency for well-conditioned echo acquisition.

III. MEASUREMENT RESULTS

Fig. 7 shows the measurement setup. The circuit system consisted of a single-element ultrasonic transducer (V310, Olympus), a FPGA (Artix7, Xilinx), a DCO (LTC6903, Analog Devices) on the FPGA board, a pulser-receiver ASIC of [28], a DC-DC converter (LT1945, Analog Devices) on the ASIC board, and an ADC (AD9214, Analog Devices). The output frequency of DCO can be programmed with a serial-port interface, and its frequency resolution around the center frequency was 10 kHz. The phantom model (Model 040GSE, CIRS) supported dual acoustic mediums with attenuation

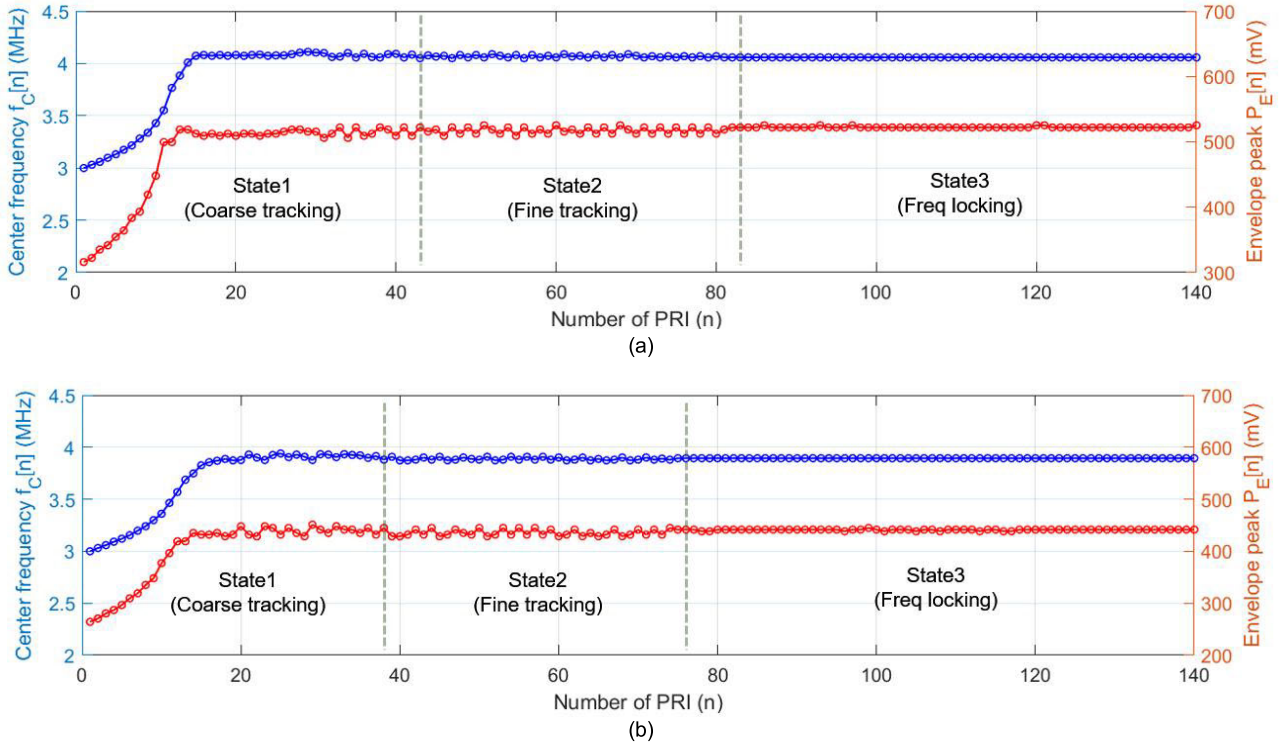

FIGURE 8. Measured center frequency value $f_C[n]$ and peak envelope $P_E[n]$ for attenuation coefficients of (a) 0.5 dB/(MHz · cm) and (b) 0.7 dB/(MHz · cm).

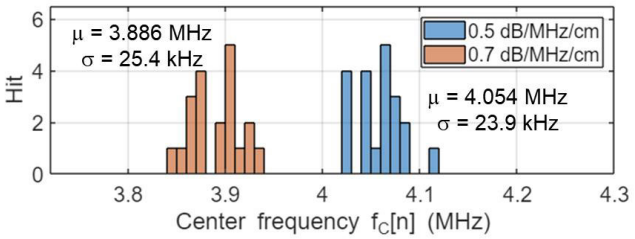

FIGURE 9. Histogram of measured center frequencies at steady state for attenuation coefficients of 0.5 and 0.7 dB/(MHz · cm).

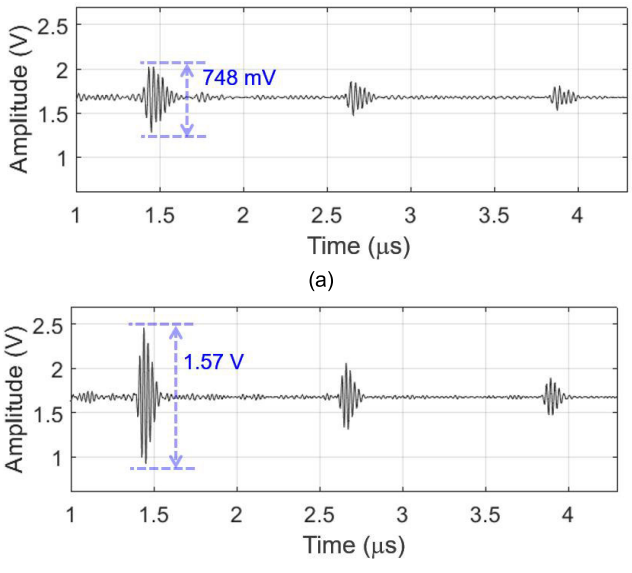

FIGURE 10. Measured A-mode waveforms at (a) initial state and (b) steady state.

coefficients of 0.5 and 0.7 dB/(MHz · cm). We used both mediums of phantom model for demonstration of proposed center frequency tracking scheme.

The FPGA part of Fig. 5 was implemented with a hardware description language (HDL) of Verilog. A summary of FPGA resource utilization is presented in Table 1. The utilization percentage of look-up-tables (LUTs) and digital signal processing (DSP) slices were 1.74 % and 5.41 %, respectively. The primary computations in the gradient ascent algorithm were based on additions and accumulations. As a result, the utilization of primary resources in FPGA was relatively low. In addition, the core HDL of this work can be implemented in ASIC if necessary.

As is well known, the transducer can be modelled as an equivalent circuit, based on the Butterworth-Van Dyke model [29]. The equivalent circuit has two arms: a mechanical arm and an electric arm. The electric arm can be simplified as a capacitance C_0. The mechanical arm is comprised of a mechanical compliance C_1, a mass component L_1, and a mechanical loss resistance R_1. In this work, these parameters were extracted with an impedance analyzer (IM7581, HIOKI), and are summarized in Table 2. The parameters in Table 2 included parasitic components of interface circuits. This work did not employ an impedance matching, because it belonged to the low-power low-Q factor transducer compared with other high-power dedicated applications [30].

The equivalent impedance of transducer can be affected by overall interface conditions such as an acoustic loading, parasitic components of interface circuits, and actuation conditions. Considering the overall interface conditions of transducer, the equivalent admittance was 0.17 + 0.00144j for the acoustic medium of 0.5 dB/(MHz · cm). The resonant frequency f_r of Table 2 was estimated by using the frequency ratio function of [11], and it was considered as the theoretical center frequency of this work. The parameters of mechanical arm for both acoustic mediums were different, and the resonant frequency was lowered for more lossy medium [6], [9], [20].

Fig. 8 shows the measured center frequency value $f_C[n]$ and peak envelope $P_E[n]$. The horizontal axis of Fig. 8 corresponds to a number of PRI, and the used PRI time is 1- ms. The blue-colored center frequency value $f_C[n]$ follows the left vertical axis, and the red-colored peak envelope $P_E[n]$ follows the right vertical axis. Fig. 8(a) and Fig. 8(b) represent the transient waveforms for acoustic mediums of 0.5 and 0.7 dB/(MHz · cm), respectively. When the A-mode scanner started to operate with the global reset, the state automatically became the State1, *Coarse tracking*, which followed the momentum based gradient ascent algorithm. When the center frequency $f_C[n]$ was almost settled, then the $P_E[n]$ was dithered with small variation. As the momentum value became small enough, the state was altered to the State2, *Fine tracking*, which tracked the center frequency with basic gradient-based algorithm. When the variation of $P_E[n]$ became further small, then the state was changed to the State3, *Freq locking*. In this state, the circuit system kept the tracked center frequency $f_C[n]$ if the variation of $P_E[n]$ was within the pre-determined tolerance. As shown in Fig. 8, the deviation of $P_E[n]$ was not zero due to measurement noise, even though the value $f_C[n]$ was constant. Noise such as aperiodic ripple of DC-DC converter could affect the operation of frequency tracking. Nonetheless, the frequency tracking results showed consistent operations. The measured average number of PRIs for steady state was 80 in this work.

Fig. 9 shows the histogram of measured center frequencies for two acoustic mediums. The repetitive measurements were performed 30 times for each of mediums. The measured mean (μ) and standard deviation (σ) values for acoustic medium of attenuation coefficient 0.5 dB/(MHz · cm) were 4.054 MHz and 23.9 kHz, respectively. The mean value of center frequency is almost the same as the optimal center frequency of envelope response of Fig. 3(a). Also, the μ and σ values for medium of attenuation coefficient 0.7 dB/(MHz · cm) were 3.886 MHz and 25.4 kHz, respectively. These results demonstrate the adaptive frequency tracking performance of the implemented A-mode scanner for different acoustic mediums. As mentioned before, the optimum center frequency for acoustic medium with attenuation coefficient of 0.7 dB/(MHz · cm) was lower than that from a medium with attenuation coefficient of 0.5 dB/(MHz · cm). Besides, the center frequency can be further changed depending on the actuation conditions such as a pulse shape, a number of pulses, and an actuation power. The absolute errors of center frequency for mediums with attenuation coefficients of 0.5 and 0.7 dB/(MHz · cm) were 61.7 kHz and 44.0 kHz, respectively. Since the Q factor of target transducer was low, a derivative of $\partial P_E/\partial f_C$ was small in the vicinity of the optimal center frequency, as shown in Fig. 3(a). In addition, a resolution of ADC also resulted in a quantization of $\partial P_E/\partial f_C$. As a result, the peak-to-peak deviation of $P_E[n]$ value at steady state was 16.1 mV for repetitive measurements. Besides, the standard deviation of $P_E[n]$ for repetitive measurements was 3.2 mV, which is a relatively small value. Note that the estimated standard deviations of frequency tracking results correspond to the tracking variance for 30 repetitive measurements. Overall, regarding the Q factor of used transducer, the error value for center frequency tracking can be considered as relatively small. Besides, the small standard deviation values demonstrate the consistent performance of the frequency tracking scheme.

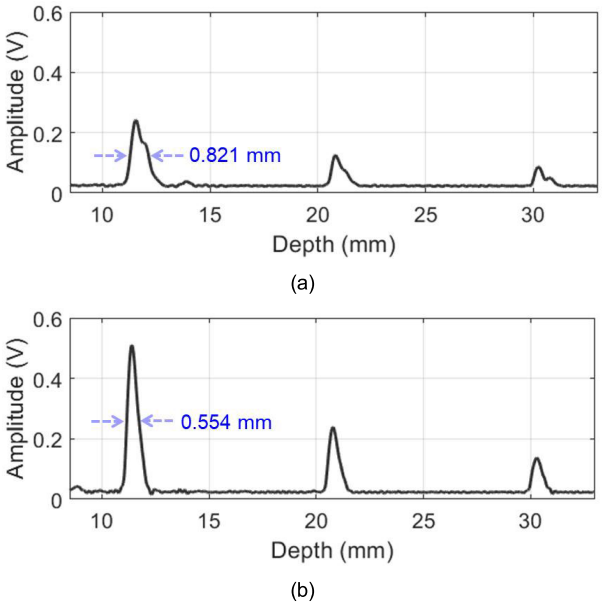

FIGURE 11. Measured envelope waveforms at (a) initial state and (b) steady state.

Fig. 10 illustrates the measured A-mode waveforms at the initial state and the steady state, respectively. The transducer was actuated with a number of cycles of 2 at a center frequency of $f_C[n]$. As illustrated in Fig. 8, the amplitude of echo signal in Fig. 10 was gradually increased as the center frequency $f_C[n]$ approaches the optimal value. In other words, the maximized amplitude of echo signal with suppressed noise means that a SNR of echo signal is also maximized. So, we evaluated an SNR of A-mode echo signal by regarding an echo packet with the highest amplitude in a single PRI as a signal and an echo from a non-scattering depth as a noise. As shown in Fig. 10, the signal amplitude was increased by 2.1 times, and the resultant SNR increment was 7.4 dB.

Fig. 11 shows the measured envelope waveforms at the initial state and the steady state, respectively. Note that we implemented the envelope detection with a combination of

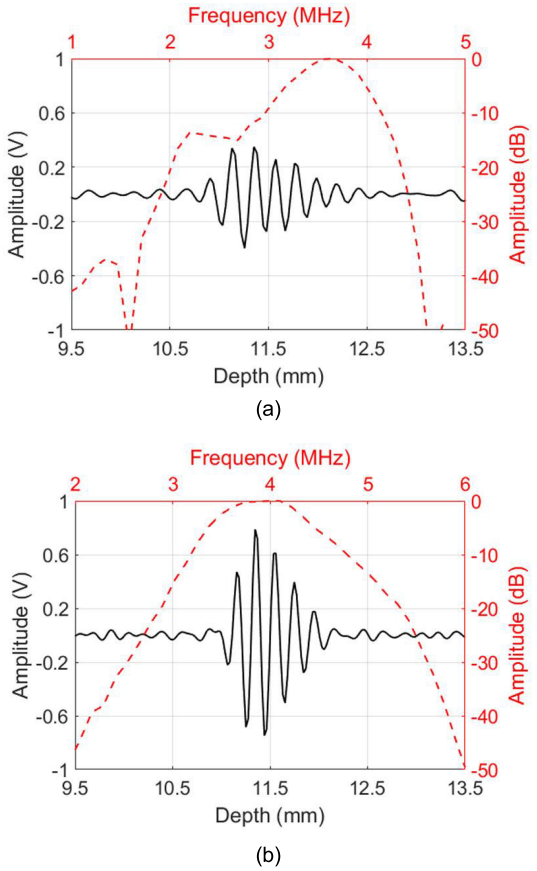

FIGURE 12. Measured pulse-echo response and frequency spectrum at (a) initial state and (b) steady state.

an absolute-value conversion and a low pass filter for low complexity of hardware. As a result, the envelope amplitude was attenuated compared with the amplitude of A-mode echo signal. We evaluated the axial resolution with the measured envelope waveforms. The axial resolutions at the initial state and the steady state were 0.821 mm and 0.554 mm, respectively. As the pulse-echo response was optimized, the axial resolution was also improved.

Fig. 12 illustrates the measured pulse-echo responses along with each of frequency spectrums at the initial state and the steady state, respectively. The center frequency at the initial state was 3.67 MHz, and the −6dB fractional bandwidth was 20 %. After executing the center frequency tracking, the center frequency at the steady state was 4.10 MHz, and the −6dB fractional bandwidth was 27 %. As the center frequency was optimized, the fractional bandwidth became more broaden. The center frequency tracking of this work not only improves the actuation efficiency but also enhances the signal-conditioning ability for an echo signal. As shown in Fig. 6, the fractional passband of BPF can be well overlapped with that of transducer when the center frequency is optimally tracked. The frequency spectrum of Fig. 12(b) also demonstrates the optimized response from actuation to acquisition including echo-signal conditioning.

Overall, the proposed center frequency tracking scheme accomplishes the optimal performances of a pulse-echo response, a maximized SNR, and an enhanced axial resolution. In addition, compared with the previous frequency tracking schemes, the work does not need additional current sensors and dedicated instruments. In details, the focus of most of previous frequency tracking schemes is oriented to the actuation conditions such as a phase difference between actuation voltage and current [6], [7], [8], [9], [10], [11]. On the other hand, the work of this paper focuses on an optimization of overall response from the transmission to the acquisition with dedicated circuit system without additional instruments.

IV. CONCLUSION

This paper proposes a center frequency tracking scheme for ultrasonic A-mode scanner circuit system. Most of previous resonant frequency tracking methods were related to high-Q-factor high-power continuous actuation applications. These works usually relied on a monitoring of phase difference between actuation voltage and current by using voltage and current sensors. On the other hand, this work deals with an optimization of center frequency for a low-Q-factor low-power pulsed actuation application without additional monitoring sensors. The proposed center frequency tracking scheme monitors the peak envelope for every PRI duration, and adjusts the center frequency value by using the momentum based gradient ascent algorithm. The employed momentum based gradient ascent algorithm has a merit of robust optimization to avoid the non-strongly concave points in a cost function. Meanwhile, the momentum based gradient method can result in a dithering around the optimal point. In this work, a gradient-ascent-algorithm based FSM is adopted to selectively use the gradient-based methods. That is, a state of coarse frequency tracking is proceeded by means of the momentum based gradient ascent algorithm. In the vicinity of the optimal center frequency, a state of fine frequency tracking is proceeded with basic gradient method.

The proposed center frequency tracking was implemented in FPGA with HDL of Verilog. The FPGA was assembled with other circuits to implement a stand-alone A-mode scanner circuit system. We performed repetitive measurements of frequency tracking for different acoustic mediums. The measurement results show the consistent tracking of center frequency for each of acoustic mediums. The average value of center frequency for a medium of 0.5 dB/(MHz · cm) attenuation coefficient was 4.054 MHz with standard deviation of 23.9 kHz. The average error of center frequency tracking was 61.7 kHz, which can be regarded as a relatively small value considering a Q factor of the utilized transducer. In addition, when the center frequency was optimally tracked, an SNR, an axial resolution, and a spectrum of pulse-echo response were also improved. Therefore, the proposed center frequency tracking can optimize the overall performance of pulse-echo response from actuation to acquisition.

ACKNOWLEDGMENT

The EDA tools were supported by IDEC, South Korea.

REFERENCES

[1] B. Jana, R. Biswas, P. K. Nath, G. Saha, and S. Banerjee, "Smartphone-based point-of-care system using continuous-wave portable Doppler," *IEEE Trans. Instrum. Meas.*, vol. 69, no. 10, pp. 8352–8361, Oct. 2020.

[2] J. He, H. Luo, J. Jia, J. T. W. Yeow, and N. Jiang, "Wrist and finger gesture recognition with single-element ultrasound signals: A comparison with single-channel surface electromyogram," *IEEE Trans. Biomed. Eng.*, vol. 66, no. 5, pp. 1277–1284, May 2019.

[3] J. Hitomi, Y. Murai, H. J. Park, and Y. Tasaka, "Ultrasound flow-monitoring and flow-metering of air–oil–water three-layer pipe flows," *IEEE Access*, vol. 5, pp. 15021–15029, 2017.

[4] P. M. Nabeel, J. Jayaraj, K. Srinivasa, S. Mohanasankar, and M. Chenniappan, "Bi-modal arterial compliance probe for calibration-free cuffless blood pressure estimation," *IEEE Trans. Biomed. Eng.*, vol. 65, no. 11, pp. 2392–2404, Nov. 2018.

[5] K. Kim, S. G. Jang, H. G. Lim, H. H. Kim, and S.-M. Park, "Acoustic power transfer using self-focused transducers for miniaturized implantable neurostimulators," *IEEE Access*, vol. 9, pp. 153850–153862, 2021.

[6] Y. Kuang, Y. Jin, S. Cochran, and Z. Huang, "Resonance tracking and vibration stablilization for high power ultrasonic transducers," *Ultrasonics*, vol. 54, no. 1, pp. 187–194, Jan. 2014.

[7] J.-D. Wang, J.-J. Jiang, F.-J. Duan, F.-M. Zhang, W. Liu, and X.-H. Qu, "A novel fast resonance frequency tracking method based on the admittance circle for ultrasonic transducers," *IEEE Trans. Ind. Electron.*, vol. 67, no. 8, pp. 6864–6873, Aug. 2020.

[8] X. Liu, A. I. Colli-Menchi, J. Gilbert, D. A. Friedrichs, K. Malang, and E. Sánchez-Sinencio, "An automatic resonance tracking scheme with maximum power transfer for piezoelectric transducers," *IEEE Trans. Ind. Electron.*, vol. 62, no. 11, pp. 7136–7145, Nov. 2015.

[9] S. Di, W. Fan, and H. Li, "Parallel resonant frequency tracking based on the static capacitance online measuring for a piezoelectric transducer," *Sens. Actuators A, Phys.*, vol. 270, pp. 18–24, Feb. 2018.

[10] J. Zhang, K. Ma, J. Wang, P. Feng, and S. Ahmad, "A fast and accurate frequency tracking method for ultrasonic cutting system via the synergetic control of phase and current," *IEEE Trans. Ultrason., Ferroelectr., Freq. Control*, vol. 69, no. 2, pp. 902–910, Feb. 2022.

[11] H. Zhang, F. Wang, Y. Tian, X. Zhao, D. Zhang, and L. Han, "Electrical matching of low power piezoelectric ultrasonic transducers for micro-electronic bonding," *Sens. Actuators A, Phys.*, vol. 199, pp. 241–249, Sep. 2013.

[12] J. Choi, S. Youn, J. Y. Hwang, S. Ha, C. Kim, and M. Je, "Energy-efficient high-voltage pulsers for ultrasound transducers," *IEEE Trans. Circuits Syst. II, Exp. Briefs*, vol. 68, no. 1, pp. 19–23, Jan. 2021.

[13] K. Chen, H.-S. Lee, A. P. Chandrakasan, and C. G. Sodini, "Ultrasonic imaging transceiver design for CMUT: A three-level 30-Vpp pulse-shaping pulser with improved efficiency and a noise-optimized receiver," *IEEE J. Solid-State Circuits*, vol. 48, no. 11, pp. 2734–2745, Nov. 2013.

[14] M. Tan, C. Chen, Z. Chen, J. Janjic, V. Daeichin, and Z.-Y. Chang, "A front-end ASIC with high-voltage transmit switching and receive digitization for 3-D forward-looking intravascular ultrasound imaging," *IEEE J. Solid-State Circuits*, vol. 53, no. 8, pp. 2284–2297, Aug. 2018.

[15] G. Jung, C. Tekes, A. Pirouz, F. L. Degertekin, and M. Ghovanloo, "Supply-doubled pulse-shaping high voltage Pulser for CMUT arrays," *IEEE Trans. Circuits Syst. II, Exp. Briefs*, vol. 65, no. 3, pp. 306–310, Mar. 2018.

[16] K.-J. Choi, H. G. Yeo, H. Choi, and D.-W. Jee, "A 28.7V modular supply multiplying pulser with 75.4% power reduction relative to CV^2f," *IEEE Trans. Circuits Syst. II, Exp. Briefs*, vol. 68, no. 3, pp. 858–862, Mar. 2021.

[17] E. Shin, H. G. Yeo, A. Yeon, C. Jin, W. Park, S.-C. Lee, and H. Choi, "Development of a high-density piezoelectric micromachined ultrasonic transducer array based on patterned aluminum nitride thin film," *Micromachines*, vol. 11, no. 6, p. 623, Jun. 2020.

[18] K. Chen, H.-S. Lee, and C. G. Sodini, "A column-row-parallel ASIC architecture for 3-D portable medical ultrasonic imaging," *IEEE J. Solid-State Circuits*, vol. 51, no. 3, pp. 738–751, Mar. 2016.

[19] J. Wang, S. H. Pun, Y. Yu, Y. Liu, C.-H. Cheng, K. F. Lei, S. Zhang, P. U. Mak, and M. I. Vai, "Use of supporting post width to increase the CMUT's resonant frequency," *IEEE Access*, vol. 10, pp. 59219–59227, 2022.

[20] M. Olfatnia, Z. Shen, J. M. Miao, L. S. Ong, T. Xu, and M. Ebrahimi, "Medium damping influences on the resonant frequency and quality factor of piezoelectric circular microdiaphragm sensors," *J. Micromech. Microeng.*, vol. 21, no. 4, Feb. 2011, Art. no. 045002.

[21] J.-Y. Jeong, J.-K. Song, M.-S. Choi, S.-K. Hong, and O.-K. Kwon, "A high frame rate analog front-end IC with piezoelectric micromachined ultrasound transducers using analog multi-line acquisition for ultrasound imaging systems," *IEEE Access*, vol. 9, pp. 119298–119309, 2021.

[22] W. Tao, G.-W. Wu, and Q. Tao, "Momentum acceleration in the individual convergence of nonsmooth convex optimization with constraints," *IEEE Trans. Neural Netw. Learn. Syst.*, vol. 33, no. 3, pp. 1107–1118, Mar. 2022.

[23] Z. Luo, S. Chen, and Y. Qian, "Stochastic momentum method with double acceleration for regularized empirical risk minimization," *IEEE Access*, vol. 7, pp. 166551–166563, 2019.

[24] Y. Guan, Y. Fu, L. Chen, G. Liu, and L. Sun, "Belief-rule-base inference method based on gradient descent with momentum," *IEEE Access*, vol. 9, pp. 34487–34499, 2021.

[25] C. Xu, Z. Peng, X. Hu, W. Zhang, L. Chen, and F. An, "FPGA-based low-visibility enhancement accelerator for video sequence by adaptive histogram equalization with dynamic clip-threshold," *IEEE Trans. Circuits Syst. I, Reg. Papers*, vol. 67, no. 11, pp. 3954–3964, Nov. 2020.

[26] S. Boyd and L. Vandenberghe, *Convex Optimization*. Cambridge, U.K.: Cambridge Univ. Press, 2009.

[27] N. Qian, "On the momentum term in gradient descent learning algorithms," *Neural Netw.*, vol. 12, no. 1, pp. 145–151, 1999.

[28] H.-T. Park and J.-Y. Um, "A programmable pulser-receiver circuit for single transducer medical ultrasound system," *J. Integr. Circuits Syst.*, vol. 7, no. 4, pp. 33–38, Oct. 2021.

[29] D. Popovici, A. Gheorghe, F. I. Hantila, and F. Constantinescu, "Modeling and simulation of piezoelectric devices," in *Modeling and Simulation*. Rijeka, Croatia: InTech, 2008, pp. 493–495.

[30] H. Zhang, F. Wang, D. Zhang, Y. Hou, and T. Xi, "A new automatic resonance frequency tracking method for piezoelectric ultrasonic transducers used in thermosonic wire bonding," *Sens. Actuators A, Phys.*, vol. 235, pp. 140–150, Oct. 2015.

DOO-HYEON KO is currently pursuing the B.S. degree with the Department of Medical IT Convergence Engineering, Kumoh National Institute of Technology, Gumi, South Korea.

His research interest includes digital systems for biomedical applications.

YOUNG-CHAN LEE received the B.S. degree from the Department of Electronic Engineering, Hannam University, Deajeon, South Korea, in 2022. He is currently pursuing the M.S. degree with the Department of Medical IT Convergence Engineering, Kumoh National Institute of Technology, Gumi, South Korea.

His research interest includes digital systems for biomedical applications.

JI-YONG UM (Member, IEEE) received the B.S., M.S., and Ph.D. degrees from the Department of Electronic and Electrical Engineering, Pohang University of Science and Technology (POSTECH), Pohang, South Korea, in 2006, 2008, and 2013, respectively

From 2014 to 2016, he was a Senior Engineer at SK Hynix, South Korea. From 2016 to 2021, he was an Assistant Professor at the Department of Electronic Engineering, Hannam University, Daejeon, South Korea. In 2021, he joined the Faculty of the Kumoh National Institute of Technology, where he is currently an Assistant Professor with the Department of Medical IT Convergence Engineering. His research interests include biomedical circuits and systems for medical ultrasound and physiological signal instrumentations.